INCORPORATION OF ALUMINUM AND IRON INTO THE ZSM-12 ZEOLITE: SYNTHESIS AND CHARACTERIZATION OF ACID SITES

Gabriela KOŠOVÁ[1] and Jiří ČEJKA[2,*]

J. Heyrovský Institute of Physical Chemistry, Academy of Sciences of the Czech Republic, Dolejškova 3, 182 23 Prague 8, Czech Republic; e-mail: [1] gabriela.kosova@jh-inst.cas.cz, [2] jiri.cejka@jh-inst.cas.cz

Received July 25, 2002
Accepted October 10, 2002

Zeolite ZSM-12 with aluminum and iron in the framework was synthesized in a broad range of Si/Al (Si/Fe) ratios using triethylmethylammonium bromide as structure-directing agent with the aim to characterize the type and concentration of acid sites in dependence on the Si/Al (Si/Fe) ratio and calcination procedure. It was shown that the minimum Si/Al ratio achieved for (Al)ZSM-12 is around 35, which is very close to the minimum Si/Fe ratio *ca* 37 for (Fe)ZSM-12. The rate of crystallization of (Al)ZSM-12 and (Fe)ZSM-12 depends on the concentration of Al and Fe in the reaction mixture. The higher was the concentration of these trivalent cations, the slower was the apparent crystallization rate. It is suggested that the crystallization rate is controlled by the number of nucleation centers, which depends on the amount of trivalent cations (Al, Fe) in the reaction mixture. Zeolites (Al)ZSM-12 and (Fe)ZSM-12 were calcined under a variety of carefully controlled conditions to investigate the resulting concentration of Brønsted and Lewis acid sites. FTIR spectroscopy used to study the adsorption of acetonitrile-d_3 and pyridine on Brønsted and Lewis acid sites revealed that both sites are present in significant concentrations in all calcined (Al)ZSM-12 and (Fe)ZSM-12 zeolites. The highest concentrations of Brønsted sites especially at low Si/Al or Si/Fe ratios were achieved *via* calcination of the zeolites in a stream of ammonia followed by a repeated sodium ion exchange and further calcination in a stream of air.

Keywords: Zeolites; Molecular sieves; ZSM-12; Aluminum; Iron; Framework incorporation; Acid sites characterization; Adsorption; IR spectroscopy.

Zeolites and other types of microporous and mesoporous molecular sieves have been intensively investigated in the recent decades in many laboratories around the world and currently are industrially used in a high number of acid-catalyzed reactions due to their strong acidity and shape-selective properties. At present, the attention is mainly paid to new ways of their synthesis[1–3], detailed understanding of their properties using both experimental[4–6] and theoretical[7,8] approaches and, last but not least, to their applications in catalysis[9–11]. This results in the continuously increasing number of catalytic applications of zeolites in large-scale processes[12]. The

main reasons for the use of zeolites in these reactions stem from their following properties: (i) well-defined inorganic crystalline structures with a variety of structural possibilities differing in channel diameters and their connectivity, (ii) a precisely defined inner volume with high surface areas up to 1000 m^2/g, (iii) the ability to concentrate molecules in the inner volume, (iv) shape selectivity, which is controlled by the relationship between the kinetic diameter of molecules and the pore dimensions and, last but not least, (v) environmental tolerance[13,14].

It is evident that the acid strength and concentration of active sites play a very important role in the catalytic performance of zeolites and, thus, the possibility to prepare zeolites with a given type and number of acid sites is highly required[9,14,15]. The concentration and acid strength distribution can be varied with the aluminum content in the synthesis mixture or even further changed by various dealumination procedures. In the case of zeolites, the concentration of Lewis sites usually increases with temperature of calcination or activation; a number of examples can be found in the literature describing the negative role of these sites in deactivation of zeolites, *e.g.* ref.[16] To characterize the amount and different types of acid sites, temperature-programmed desorption is usually used; however, this technique does not allow to distinguish between Brønsted and Lewis acid sites. For this reason infrared spectroscopy is advantageously used in combination with the adsorption of proper probe molecules like acetonitrile-d_3 or pyridine[17,18].

The objective of this contribution is to describe the optimum synthesis procedure for aluminum- and iron-containing ZSM-12 with a different range of Si/Al and Si/Fe ratios, to characterize in detail the kinetics of crystallization and to explain the role of calcination procedures for the final concentration of the individual types of acid sites. Zeolite ZSM-12 belongs to high-silica zeolites with one-dimensional pore structure consisting of linear, non-penetrating channels formed by 12-membered rings with a diameter of about 0.57 × 0.61 nm. Zeolite ZSM-12 was originally synthesized by Rosinsky and Rubin[19] and synthesis of this zeolite was described in detail by Ernst *et al.*[20] ZSM-12 can be synthesized in the range of Si/Al ratio from about 25 up to at least 100 and it seems that the optimum template for its synthesis is triethylmethylammonium bromide while in the case of tetraethylammonium bromide zeolites ZSM-5 and Beta can be simultaneously formed[21]. The first proposal of the structure of ZSM-12 was given by LaPierre *et al.*[22], which was further refined by Fyfe *et al.*[23] Finally, this structure was confirmed by a high-resolution transmission electron microscopy by Ritsch *et al.*[24] Recently, syntheses of ZSM-12 in the form of supported films and membranes were also described[25].

Catalytic properties of this zeolite were investigated *e.g.* in cumene synthesis by benzene alkylation with propene or isopropyl alcohol[26,27]. In addition, Zhang and Smirniotis[28] described superior time-on-stream stability of zeolite ZSM-12 in reforming of naphthenic hydrocarbons due to the limitation of coke formation. A possible application of zeolite ZSM-12 as an oxidation catalyst was demonstrated by Reddy *et al.*[29] and Bhaumik *et al.*[30] for vanadium-containing ZSM-12 in phenol oxidation and alkane, cycloalkane and ethylbenzene oxidation, respectively, and phenol, cresol and xylene oxidation over tin-containing ZSM-12 by Mal *et al.*[31]

EXPERIMENTAL

Materials

The following reagents were used in the synthesis of (Al)ZSM-12 and (Fe)ZSM-12 zeolites: aluminum nitrate (Fluka), ferric nitrate (Fluka), sulfuric acid (Lachema), sodium silicate (Riedel de Haën) and triethylmethylammonium bromide (Aldrich).

Synthesis

For hydrothermal synthesis of zeolites (Al)ZSM-12 and (Fe)ZSM-12 with different Si/Al and Si/Fe ratios, triethylmethylammonium bromide (TEMABr) as a structure-directing agent was used. The reaction mixture was prepared in a polypropylene beaker at ambient temperature. In a typical synthesis, 1.33 g of $Al(NO_3)_3 \cdot 9H_2O$ was dissolved in 37.6 g of distilled water followed by addition of 2.8 g H_2SO_4. Then 31.6 g of sodium silicate in 37.6 g of distilled water was added under vigorous stirring. The mixture was stirred for 60 min. Afterwards, 11.52 g of organic template TEMABr was dissolved in 37.6 g of distilled water and added to the reaction gel, which was finally homogenized for another 60 min. The reaction gel was loaded into a 35 ml Teflon-lined stainless steel autoclave. The synthesis was carried out under static conditions at 140 °C under autogenous pressure. To study the kinetics of the synthesis, the reaction time was varied between 12 and 300 h. The same reaction procedure was used for the synthesis of (Fe)ZSM-12 in which aluminum nitrate was replaced by ferric nitrate. After crystallization, the autoclaves were cooled down to room temperature by quenching in water, the solid product was recovered by filtration, washed with distilled water and dried at 100 °C for 5 h.

Calcination Procedures

To investigate the effect of template removal from the as-synthesized zeolites on the type and concentration of acid sites, the following four different calcination procedures were carefully performed:

1. Zeolites (Al)ZSM-12/1 were calcined at 550 °C for 8 h in a stream of air with a temperature ramp of 1 °C/min.

2. Zeolites (Al)ZSM-12/2 were calcined at 500 °C for 32 h in a stream of air with the same temperature ramp.

3. Zeolites (Al)ZSM-12/3 were calcined at 350 °C for 2 h in a stream of air, then the zeolite was cooled down to the ambient temperature followed by twice repeated ion-exchange with 0.5 M $NaNO_3$ for 8 h and one with 1 M $NaNO_3$ for 8 h using 100 ml of nitrate solution per 1 g of zeolite. After that zeolites were calcined at 550 °C for 8 h (temperature ramp 1 °C/min).

4. Zeolites (Al)ZSM-12/4 were calcined at 460 °C for 4 h in a stream of ammonia, then the samples were ion-exchanged twice with 0.5 M $NaNO_3$ for 8 h, once with 1 M $NaNO_3$ for 8 h using 100 ml of solution for 1 g of zeolite at room temperature and calcined again at 550 °C for 8 h in a stream of air (temperature ramp 1 °C/min).

Only procedures *1* and *4* were applied to calcine (Fe)ZSM-12 zeolites.

Prior to the characterization of acid sites the, ammonium forms of all ZSM-12 zeolites were prepared *via* four-times repeated ion exchange with 0.5 M ammonium nitrate at ambient temperature (100 ml of solution for 1 g of zeolite, 4 h). After the ion exchange, the zeolites were washed thoroughly with distilled water and dried at 50 °C for 5 h.

Instrumentation

X-Ray powder diffraction was used for the identification of synthesized zeolite, quantification of their crystallinity and to follow the kinetics of crystallization of zeolites (Al)ZSM-12 and (Fe)ZSM-12. The XRD patterns were collected with a Siemens D5005 powder X-ray diffractometer equipped with graphite monochromator and scintillation counter using CuKα radiation in Bragg–Brentano geometry. To determine the relative crystallinity of the zeolites after different synthesis times, the relative intensity of the peak of $2\theta = 20.99°$ was used and compared to that of the best crystalline ZSM-12 obtained in this study.

The shape and size of zeolite crystals were determined by scanning electron microscopy (JEOL, JSM-03). To estimate the chemical composition of synthesized (Al)ZSM-12 and (Fe)ZSM-12, X-ray fluorescence spectroscopy was employed.

FTIR spectra of zeolites were recorded on a FTIR spectrometer Nicolet Protégé 460 with an MTC/A detector. The IR spectra of skeletal vibrations were recorded using the KBr pellet technique[32]. The concentrations of Brønsted and Lewis acid sites in (Al)ZSM-12 and (Fe)ZSM-12 zeolites were determined after adsorption of acetonitrile-d_3 and pyridine, respectively, followed by FTIR spectroscopy. For this purpose, zeolite powders were pressed binder-free into self-supporting wafers with a density of 8.0–11.0 mg/cm^2. Acetonitrile and pyridine were degassed by repeating freezing and thawing cycles before use. The concentrations of Lewis (L) and Brønsted (B) sites in (Al)ZSM-12 zeolites were determined after adsorption of acetonitrile-d_3, while pyridine was used for the determination of these sites in (Fe)ZSM-12, as it was reported that acetonitrile-d_3 cannot be used to distinguish Brønsted and Lewis sites in iron-containing molecular sieves[33]. Prior to the adsorption of probe molecules, zeolites ZSM-12 were activated *in situ* by overnight evacuation at 400 °C. Adsorption of acetonitrile-d_3 on activated (Al)ZSM-12 was carried out at 25 °C for 30 min while pyridine was admitted to interact with acid sites of (Fe)ZSM-12 at 170 °C at partial pressure of 750 Pa for 30 min. The adsorption in both cases was followed by evacuation for 20 min. All measured spectra were recorded at room temperature with a resolution of 2 cm^{-1} by collecting 200 scans for a single spectrum and recalculated to a normalized wafer thickness of 10 mg/cm^2. IR bands of adsorbed acetonitrile-d_3 were deconvoluted using a procedure consisting from identification of the band position in a second-derivative mode of the spectrum and least-square minimization routine approximating the bands by a Gaussian profile[17]. From integral

intensities of individual bands – the C≡N–B vibration at 2296 cm^{-1} and the C≡N–L vibration at 2323 cm^{-1} and extinction coefficients of ε(B) = 2.05 ± 0.1 cm/μmol and ε(L) = 3.6 ± 0.1 cm/μmol concentrations of Lewis and Brønsted sites were calculated according to ref.[17] To determine the concentration of Lewis acid sites, pyridine adsorbed coordinatively on electron acceptor sites, (ε_L), and concentration of Brønsted acid sites, characteristic by pyridinium ions, (ε_B), acid sites on (Fe)ZSM-12, the following extinction coefficients were used: ε_L = 1.67 ± 0.1 and ε_B = 2.22 ± 0.1 cm/μmol (ref.[34]).

RESULTS AND DISCUSSION

Kinetics of the Synthesis of (Al)ZSM-12 and (Fe)ZSM-12

Aluminum and iron ZSM-12 zeolites were readily synthesized at 140 °C from the reaction gels with the following ratios of reactant components: Na_2O:TEMABr:Al_2O_3 (Fe_2O_3):SiO_2:H_2O = 20–99:30–99:1:70–240:3000–10 300 (Table I). It should be noted that all (Fe)ZSM-12 zeolites exhibited white color, which strongly indicates that no extra-framework oxidic iron species were present in these zeolites. The optimized synthesis time for different Si/Al ratios ranged from 144 to 192 h while for different Si/Fe ratios from 168 to 216 h. Figure 1 depicts the course of the crystallization of (Al)ZSM-12

TABLE I
Synthesis of zeolites (Al)ZSM-12 and (Fe)ZSM-12 (synthesis temperature 140 °C)

Zeolite	$(Si/Al)_0$[a]	Na_2O:TEMABr:Al_2O_3:SiO_2:H_2O	Time, h
(Al)ZSM-12	35	20:30:1:70:3000	216
(Al)ZSM-12	40	22:33:1:80:3550	192
(Al)ZSM-12	60	33:48:1:120:5150	168
(Al)ZSM-12	90	50:75:1:180:7900	144
(Al)ZSM-12	120	66:99:1:240:10 300	120
Zeolite	**$(Si/Fe)_0$[a]**	**Na_2O:TEMABr:Fe_2O_3:SiO_2:H_2O**	**Time, h**
(Fe)ZSM-12	40	22:33:1:80:3550	216
(Fe)ZSM-12	60	33:48:1:120:5150	192
(Fe)ZSM-12	70	38:56:1:140:6010	192
(Fe)ZSM-12	90	50:75:1:180:7900	168

[a] $_0$ Initial.

with the Si/Al ratio in the reaction gel of 40 followed by X-ray powder diffraction. It can be clearly seen that the first diffraction lines appeared after about 96 h but still a significant amount of amorphous phase was present in this material (evidence given by a broad peak 2θ = 20–25° and SEM, not given in this paper). In the first *ca* 80 h of the synthesis, only X-ray amorphous phase was observed[35]. The best crystalline zeolite was obtained after 168 h and further increase in the synthesis time led only to slow formation of undesired cristobalite. Ernst *et al.*[20] proposed that formation of cristobalite could be avoided by lowering the pH of the reaction mixture and/or synthesis temperature. From a comparison of the time dependence of diffractograms of (Al)ZSM-12 and (Fe)ZSM-12 (*cf.* Figs 1 and 2) it is evident that the crystallization rate is higher in the case of (Al)ZSM-12. The first diffraction lines in (Fe)ZSM-12 were observed only after 120 h; to obtain a good crystalline material, at least 192 h was needed. Although it was claimed[19–21] that ZSM-12 zeolite can be synthesized in a broad range of Si/Al ratios, the increasing content of aluminum in the reaction mixture has a significant effect on the rate of crystallization. Time dependences of relative crystallinity for (Al)ZSM-12 with Si/Al ratios 40, 60 and 90 and (Fe)ZSM-12 with the same Si/Fe ratios are depicted in Figs 3 and 4. From these figures it is evident that the rate of crystallization decreases with the increasing amount of either aluminum or iron in the reaction mixture. This finding is in an agreement with the results of Ernst *et al.*[20] obtained at higher synthesis temperatures. While for (Al)ZSM-12 zeolite with the Si/Al

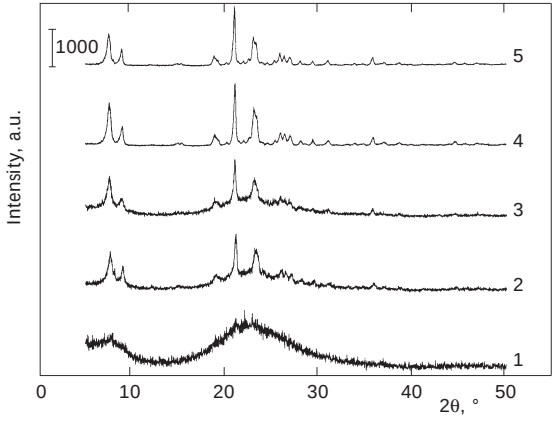

FIG. 1

X-Ray powder diffraction patterns of (Al)ZSM-12, initial Si/Al = 40, temperature of synthesis 140 °C. Crystallization time in h: 72 (1), 96 (2), 120 (3), 144 (4), 168 (5)

ratio 90, the intensity of the diffraction line at 2θ = 20.99° was at least 80%, the intensity of this peak for (Al)ZSM-12 with Si/Al ratio 40 was only about 35% (Fig. 3). In the case of (Fe)ZSM-12 it was also found that with increasing ratio Si/Fe, the rate of crystallization increases. In addition, comparing Figs 3 and 4 it is evident that incorporation of aluminum in the silicate framework of ZSM-12 proceeded much easier compared to iron. For (Fe)ZSM-12

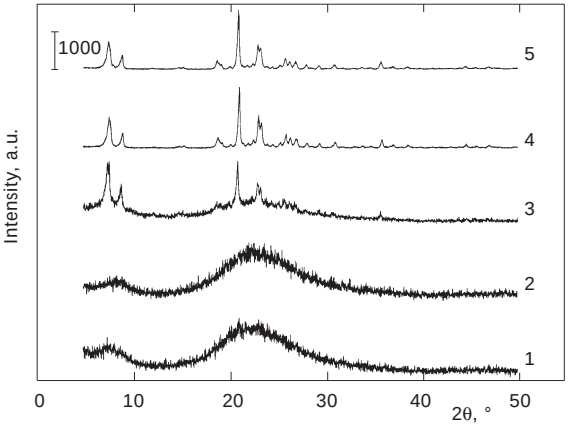

FIG. 2
X-Ray powder diffraction patterns of (Fe)ZSM-12, initial Si/Fe = 40, temperature of synthesis 140 °C. Crystallization time in h: 72 (1), 96 (2), 120 (3), 144 (4), 168 (5)

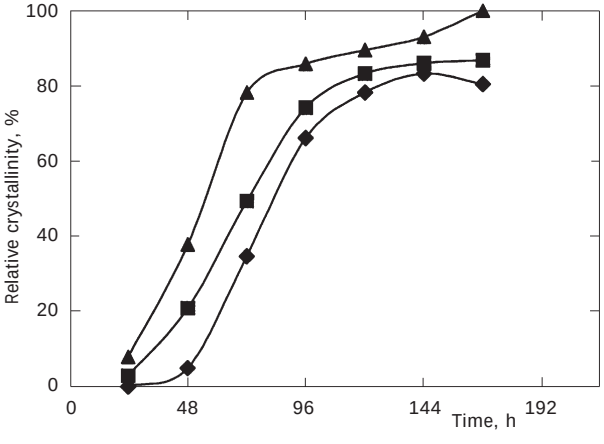

FIG. 3
The dependence of relative crystallinity of (Al)ZM-12 on the initial Si/Al ratio at 140 °C. Si/Al = 40 (◆), 60 (■) and 90 (▲)

with Si/Fe = 40, the first diffraction lines were observed after 120 h of the synthesis time.

High crystallinity of all synthesized zeolites was also confirmed by the infrared spectra of their skeletal vibrations (see Figs 5 and 6). According to the Flanigen–Khatami–Szymanski correlation[36], the absorption bands near

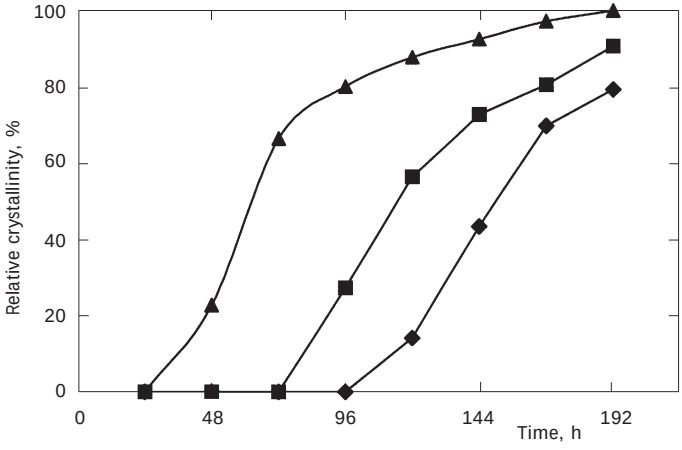

FIG. 4
The dependence of relative crystallinity of (Fe)ZM-12 on the initial Si/Fe ratio at 140 °C. Si/Fe = 40 (◆), 60 (■) and 90 (▲)

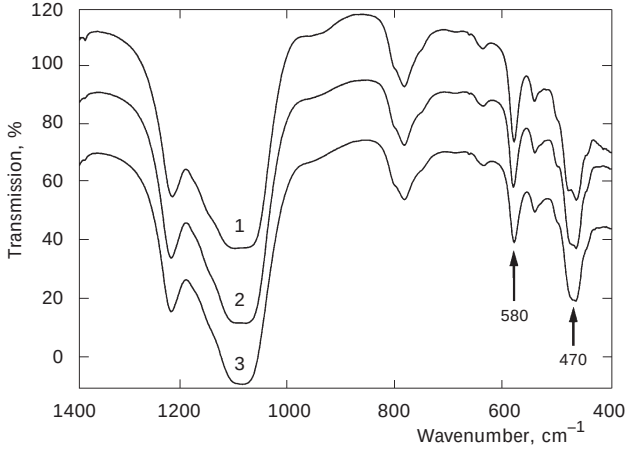

FIG. 5
Infrared spectra of skeletal vibrations of zeolite (Al)ZSM-12 with different Si/Al ratios. Si/Al = 90 (1), 60 (2) and 40 (3)

1100, 700 and 450 cm^{-1} were assigned to internal vibrations of SiO_4 or AlO_4 tetrahedra but for confirmation of the high crystallinity of this zeolite the presence of the band at 580 cm^{-1} is important. This band is usually assigned to double-four or double-six rings of tetrahedra in the framework and is usually taken as a characteristic band for high-silica ZSM-type zeolites[32]. In the case of zeolite ZSM-12, it is clearly seen that the position of this band is not influenced by the presence of aluminum or iron in the framework, which is in agreement with the assumption that the presence of this band is connected with the vibrations of some larger rings and not of individual tetrahedra.

Chemical analysis of the synthesized zeolites ZSM-12 and their mother liquids after the syntheses clearly showed that practically all aluminum or iron, given to the synthesis mixture, is present only in the solid phase. On the other hand the Si/Al ratio in the reaction gel and in the solid product differ significantly. It indicates that some portion of silicates was not incorporated into the crystalline phase of this zeolite. Figure 7 depicts the dependences of Si/Al and Si/Fe ratios in as-synthesized zeolites on these initial ratios in the synthesis mixtures. It is evident that with decreasing concentration of Al and Fe in the synthesis mixture, the amount of silicates not incorporated in the zeolite structure increases. Simultaneously with increasing aluminum or iron content, the induction period increases (*cf.* Figs 3 and 4) and prolongs the time necessary for complete crystallization. High aluminum contents also suppress the formation of the dense cristobalite

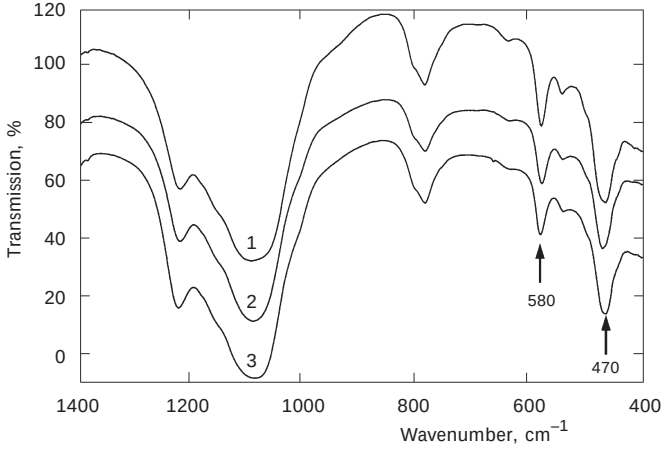

FIG. 6

Infrared spectra of skeletal vibrations of zeolite (Fe)ZSM-12 with different Si/Fe ratios. Si/Fe = 90 (1), 60 (2) and 40 (3)

impurity phase[37]. The initial Si/Al (Si/Fe) ratio in the synthesis mixture influences also the resulting size of zeolite crystals while the type of cations has an important impact on their shape. (Al)ZSM-12 crystals possess typical elongated shape ("rice-shape" crystals) and their size increases with decreasing concentration of aluminum in the reaction mixture (see Fig. 8). The maximum length of the crystals of (Al)ZSM-12 with Si/Al = 120 was about 5–6 μm. On the other hand, the crystals of (Fe)ZSM-12 are more regular and also smaller. The maximum size observed for (Fe)ZSM-12 with Si/Fe = 90 was around 3–4 μm (Fig. 9). Characteristic shapes of crystals of (Al)ZSM-12 and (Fe)ZSM-12 are compared in Fig. 10 showing rice-shaped crystals of (Al)ZSM-12 and intergrowth of individual crystals in the case of (Fe)ZSM-12.

These results indicate that the amount of aluminum (or iron) in the reaction mixture controls not only the apparent rate of crystallization but in fact is decisive for the rate of nucleation. It has been shown that the induction period is shorter with decreasing concentration of aluminum (iron) in the reaction mixture (*cf.* Figs 3 and 4). The lower is the concentration of aluminum, the shorter is the induction period. This observation can be explained on the basis of the formation of a different number of nucleation centers in the early stages of the synthesis of zeolite ZSM-12. It is expected that aluminum is very rapidly incorporated into the nucleation species and, due to its negative charge, it significantly contributes to their interaction with cationic structure-directing agents. At low aluminum concentrations, a relatively low amount of such nucleation species is formed, and

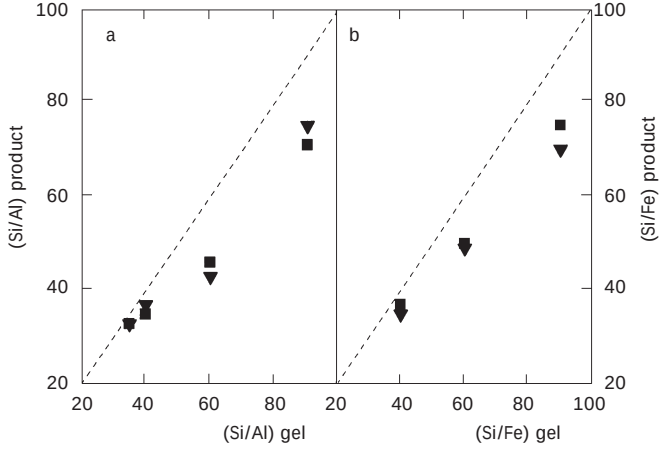

FIG. 7

The dependence of Si/Al ratio (a) and Si/Fe ratio (b) of as-synthesized zeolites (Al)ZSM-12 and (Fel)ZSM-12, respectively, on the initial Si/Al (Si/Fe) ratio. ▼, ■ – different experiments

thus, only a limited number of crystals arise. Therefore, the induction period is apparently shorter and the crystallization proceeds faster. On the other hand, with increasing amount of aluminum in the reaction mixture, the concentration of nucleation species is much higher and longer time is required to obtain X-ray-observable crystal particles. This explanation is also in line with increasing crystal size for aluminum (iron) deficit zeolite crystals.

Characterization and Modification of Acid Sites

There is no doubt that simultaneous presence of Brønsted and Lewis sites results in enhanced zeolite activity in various transformations of hydrocarbons[16,38–40]. Unfortunately, no definite conclusions have been drawn to explain this phenomenon. While some authors suggested that this is due to an increased acidity of a proton adjacent to the Al electron acceptor site,

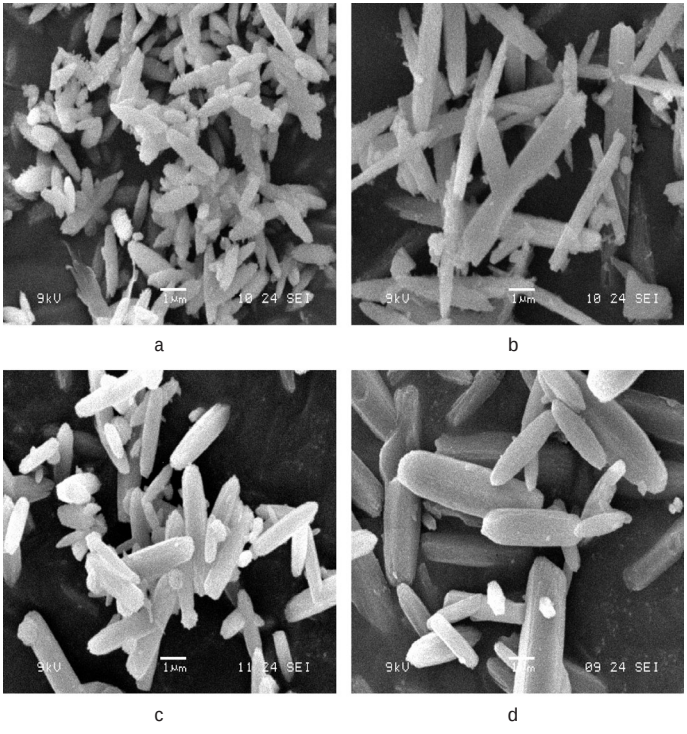

FIG. 8
Scanning electron micrographs of zeolites (Al)ZSM-12 with different initial Si/Al ratios: 40 (a), 60 (b), 90 (c), 120 (d)

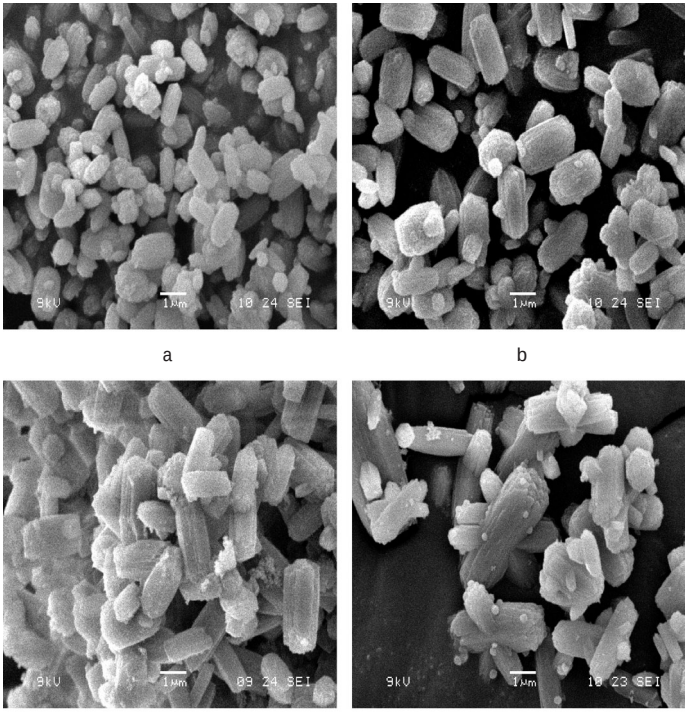

FIG. 9
Scanning electron micrographs of zeolites (Fe)ZSM-12 with different initial Si/Fe ratios: 40 (a), 60 (b), 70 (c), 90 (d)

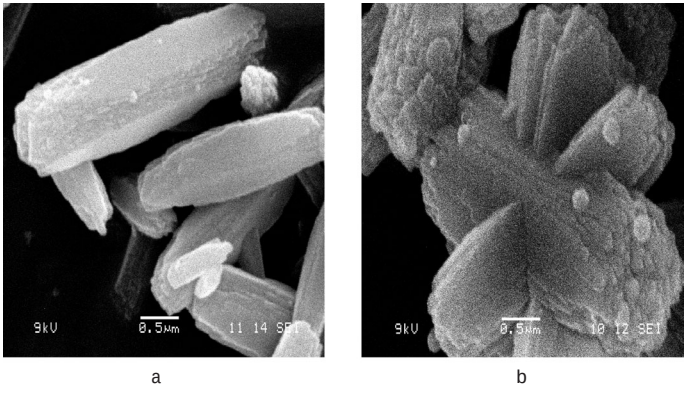

FIG. 10
Comparison of a typical shape of ZSM-12 crystals with aluminum (a) and iron (b) in the framework

others proposed synergistic function of both Brønsted and Lewis acid sites in hydrocarbon transformations. However, it is evident that the type and concentration of acid sites control the rate of acid-catalyzed reactions of hydrocarbons and their derivatives over zeolite catalysts.

In the case of (Al)ZSM-12, the IR spectra in the hydroxyl region consist of three typical bands at 3750 cm^{-1} (terminal silanol groups), and two types of bridging Si–OH–Al groups at 3610 and 3575 cm^{-1} (Fig. 11a). According to Chiche *et al.*[41], the infrared bands at 3610 and 3575 cm^{-1} can be tentatively attributed to hydroxyl groups vibrating in the main channel and in the six-membered rings of the structure, respectively. No absorption band at 3650–3670 cm^{-1} was observed in the spectrum of (Al)ZSM-12, which evidences that no Al–OH groups are present. In the case of (Fe)ZSM-12, these absorption bands exhibit maxima at 3630 and 3590 cm^{-1} (Fig. 12a). The shift of the maxima of the bridging hydroxyl groups to higher wavenumbers is connected with a change of acid strength of these OH groups and this was described also for other types of zeolites, *e.g.* refs[42,43]. It will be shown later, that both types of hydroxyl groups are accessible to acetonitrile-d_3 and pyridine molecules.

The adsorption of acetonitrile-d_3 on (Al)ZSM-12 resulted in the disappearance of both bridging OH groups originally located at 3610 and 3575 cm^{-1} and in the appearance of new absorption bands at 2330 and 2300 cm^{-1} characteristic of the stretching mode of ν(C≡N) of acetonitrile-d_3 interacting

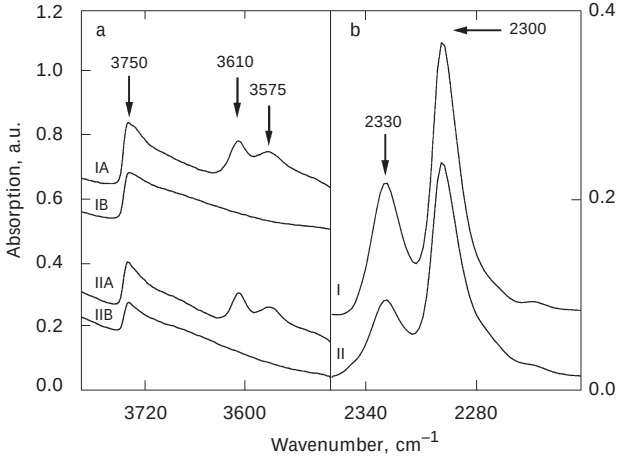

FIG. 11

The FTIR spectra of OH stretching region (a) of (Al)ZSM-12 with Si/Al = 40 (I) and 90 (II) prior to adsorption (A) and after adsorption (B) and spectra of the C≡N region of acetonitrile-d_3 after its adsorption (b)

with Lewis and Brønsted acid sites, respectively (Fig. 11a and 11b). It was described that this interaction leads to a shift of this band to higher frequencies, which makes it possible to distinguish acid sites of various nature (Lewis acid sites 2320–2330 cm^{-1}, Brønsted acid sites 2295–2300 cm^{-1})[17,44,45]. Table II depicts the concentrations of Brønsted and Lewis sites in (Al)ZSM-12 with different Si/Al ratios. It is clearly seen that all (Al)ZSM-12 zeolites possess significant amounts of Lewis acid sites and, after a typical calcination procedure, the concentration of Lewis sites is up to 40% of all acid sites, especially at low Si/Al ratios. Similar concentrations of Lewis sites in (Al)ZSM-12 were also found by Chiche *et al.*[41] in contrast to results of Zhang *et al.*[46] who reported only negligible amounts of Lewis sites in the same zeolite. To decrease the concentration of Lewis sites, other calcination procedures were tested (see Experimental). Figure 13a gives the relationship between the concentration of Brønsted and Lewis sites depending on the type of calcination procedure. While calcination at 500 °C in air with for a prolonged time as well as calcination at 450 °C followed by ion-exchange with sodium nitrate and further calcination did not change substantially the concentrations of individual sites, calcination in a stream of ammonia followed by ion-exchange with $NaNO_3$ and calcination in air was the only procedure, which led to a significant decrease in the amount of Lewis sites formed. This calcination procedure was described by Kunkeler *et al.*[47] for zeolite Beta and it was proposed that the role of structure-directing cations during the calcination is taken over by ammonium. According to

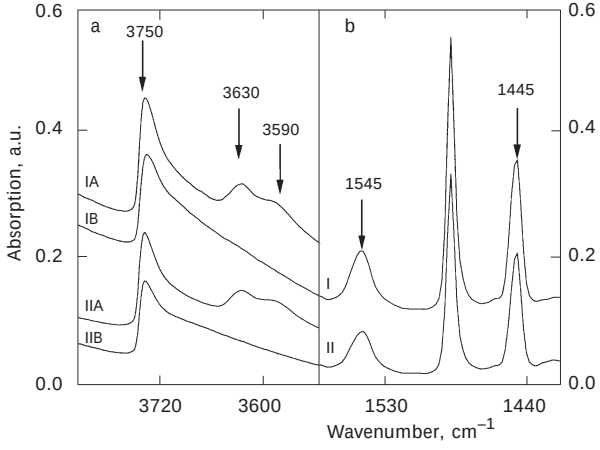

FIG. 12

The FTIR spectra of OH stretching region (a) of (Fe)ZSM-12 with Si/Fe = 40 (I) and 90 (II) prior to adsorption (A) and after adsorption (B) and spectra of adsorbed pyridine on this zeolite (b)

Bourgeat-Lami *et al.*[48], ammonium cations prevent the formation of octahedrally coordinated aluminum and partly stabilize the structure of the zeolites. After this calcination procedure, the concentration of Lewis sites significantly decreased and it was possible to achieve about 80% of Brønsted sites in (Al)ZSM-12 with Si/Al = 40. The values of Si/Al ratios calculated from quantitative interpretation of spectra of acetonitrile-d_3 are slightly higher compared to bulk chemical analysis. This is probably caused by the fact that extinction coefficients used were determined for another zeolite.

Pyridine adsorption on (Fe)ZSM-12 resulted in consumption of all bridging Si–OH–Fe groups at 3630 and 3590 cm^{-1} and in the formation of new bands at 1545 cm^{-1} (pyridine adsorption on Brønsted sites) and 1445 cm^{-1} (pyridine coordinated to Lewis sites), see Fig. 12a and 12b. This means that all acid OH groups are accessible to pyridine molecules, which indicates that the protons of OH groups tentatively assigned to hydroxyl groups located in six-membered rings (band at 3590 cm^{-1}) can interact with a base molecule like pyridine. Using the extinction coefficients by Emeis[34] the concentrations of Brønsted and Lewis sites were determined. These values (Table II) are again of about 10–20% lower compared to chemical analysis. The concentrations of Lewis sites again increase with decreasing Si/Fe ratio (Fig. 13b), which confirms that in the case of a number of high silica zeolites, the higher the concentration of trivalent atom in the framework, the higher the concentration of Lewis sites. The amount of Lewis sites in

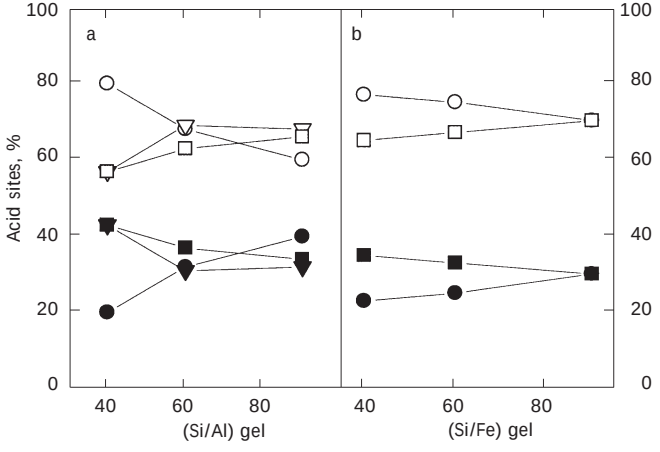

FIG. 13

Dependence of the concentration of Brønsted and Lewis sites on the Si/Al ratio in zeolite (Al)ZSM-12 (a) and on the Si/Fe ratio in zeolite (Fe)ZSM-12 (b) for different calcination procedures (see Experimental): *1*. ❑, *2*. ∇, *4*. ❍ (Brønsted sites); *1*. ■, *2*. ▼, *4*. ● (Lewis sites)

(Fe)ZSM-12 calcined under typical conditions (procedure 1) was found to be *ca* 40%. Using calcination under a stream of ammonia, the concentration of Lewis sites was limited to about 20–25%.

TABLE II
Si/Al (Si/Fe) ratios in zeolites (Al)ZSM-12 and (Fe)ZSM-12: by chemical analysis and by infrared spectroscopy after adsorption of acetonitrile-d_3 and pyridine, and concentrations of Brønsted and Lewis sites

Zeolite	$(Si/Al)_0$[a]	$(Si/Al)_p$[b]	$(Si/Al)_{IR}$	Brønsted sites[c] mmol/g	Lewis sites[c] mmol/g
(Al)ZSM-12/1	40	35	43	0.24	0.07
(Al)ZSM-12/1	60	46	49	0.20	0.06
(Al)ZSM-12/1	90	71	80	0.13	0.03
(Al)ZSM-12/2	40	35	43	0.22	0.08
(Al)ZSM-12/2	60	46	49	0.21	0.06
(Al)ZSM-12/2	90	71	77	0.15	0.03
(Al)ZSM-12/3	40	35	42	0.24	0.07
(Al)ZSM-12/3	60	46	50	0.22	0.04
(Al)ZSM-12/3	90	71	84	0.15	0.02
(Al)ZSM-12/4	40	35	37	0.35	0.04
(Al)ZSM-12/4	60	46	51	0.26	0.03
(Al)ZSM-12/4	90	71	78	0.14	0.03
Zeolite	$(Si/Fe)_0$[a]	$(Si/Fe)_p$[b]	$(Si/Fe)_{IR}$	Brønsted sites[d] mmol/g	Lewis sites[d] mmol/g
(Fe)ZSM-12/1	40	37	46	0.08	0.12
(Fe)ZSM-12/1	60	50	60	0.06	0.10
(Fe)ZSM-12/1	90	75	79	0.05	0.07
(Fe)ZSM-12/4	40	37	60	0.10	0.09
(Fe)ZSM-12/4	60	50	66	0.08	0.08
(Fe)ZSM-12/4	90	75	84	0.07	0.05

[a] $_0$ Initial; [b] $_p$ product. Adsorption of [c] acetonitrile; [d] pyridine.

CONCLUSIONS

Zeolites (Al)ZSM-12 and (Fe)ZSM-12 were synthesized in the broad range of Si/Al (Si/Fe) ratios at the temperature of 140 °C under static conditions. The rate of crystallization was controlled by the concentration of aluminum (iron) in the reaction mixture. With increasing concentration of these elements the apparent crystallization rate decreased, the time required for complete crystallization increased and the size of the zeolite crystals decreased. This was explained by the decisive role of aluminum or iron in the formation of nucleation centers and their further growth.

Incorporation of aluminum into the zeolite framework was much more easier compared to iron, which was evidenced by the significant prolongation of the synthesis time for (Fe)ZSM-12.

Acid forms of both (Al)ZSM-12 and (Fe)ZSM-12 contained significant amounts of Brønsted and Lewis sites. The concentration of Lewis sites could be substantially decreased *via* calcination of these zeolites in a stream of air followed by sodium ion-exchange. After such calcination at least 80% of aluminum formed Brønsted sites.

This study was supported by the Grant Agency of the Academy of Sciences of the Czech Republic (A4040001) and by Volkswagen-Stiftung (I/75 886). The authors also thank Dr O. Bortnovský for technical assistance in the calcinations in ammonia and Dr L. Brabec for recording the scanning electron micrographs.

REFERENCES

1. Corma A., Navarro M. T., Rey F., Rius J., Valencia S.: *Angew. Chem., Int. Ed.* **2001**, *40*, 2277.
2. Nery J. G., Hwang S.-J., Davis M. E.: *Microporous Mesoporous Mater.* **2002**, *52*, 19.
3. Kooyman P. J., Slabová M., Bosáček V., Čejka J., Rathouský J., Zukal A.: *Collect. Czech. Chem. Commun.* **2001**, *66*, 555.
4. Jaroniec M., Kruk M., Shin H. J., Ryoo R., Sakamoto Y., Terasaki O.: *Microporous Mesoporous Mater.* **2001**, *48*, 127.
5. Čejka J., Žilková N., Rathouský J., Zukal A.: *Phys. Chem. Chem. Phys.* **2001**, *3*, 5076.
6. Dědeček J., Žilková N., Čejka J.: *Collect. Czech. Chem. Commun.* **2001**, *66*, 567.
7. Spuhler P., Holthausen M. C., Nachtigallova D., Nachtigall P., Sauer J.: *Chem. Eur. J.* **2002**, *8*, 2099.
8. Nachtigall P., Davidová M., Nachtigallová D.: *J. Phys. Chem. B* **2001**, *105*, 3510.
9. Corma A.: *Chem. Rev. (Washington, D. C.)* **1997**, *97*, 2373.
10. Čejka J., Krejčí A., Žilková N., Kotrla J., Ernst S., Weber A.: *Microporous Mesoporous Mater.* **2002**, *53*, 121.
11. Perego C., Ingallina P.: *Catal. Today* **2002**, *73*, 3.
12. Tanabe K., Hölderich W. F.: *Appl. Catal., A* **1999**, *181*, 399.

13. van Bekkum H., Flanigen E. M., Jacobs P. A., Jansen J. C. (Eds): *Introduction to Zeolite Science and Practice*, 2nd ed. Elsevier, Amsterdam 2001.
14. Čejka J., Wichterlová B.: *Catal. Rev.* **2002**, *44*, 375.
15. Corma A.: *Chem. Rev. (Washington, D. C.)* **1995**, *95*, 559.
16. Wichterlová B., Žilková N., Uvarova E., Čejka J., Sarv P., Paganini C., Lercher J. A.: *Appl. Catal., A* **1999**, *182*, 297; and references therein.
17. Wichterlová B., Tvarůžková Z., Sobalík Z., Sarv P.: *Microporous Mesoporous Mater.* **1998**, *24*, 223.
18. Busca G.: *Phys. Chem. Chem. Phys.* **1999**, *1*, 723.
19. Rosinski E. J., Rubin M. K.: U.S. 3 832 449, assigned to Mobil Oil Corp. (1974).
20. Ernst S., Jacobs P. A., Martens J. A., Weitkamp J.: *Zeolites* **1987**, *7*, 458.
21. Katovic A., Giordano G. in: *Synthesis of Microporous Materials: Zeolites, Clays and Nanostructures* (M. L. Occelli and H. Kessler, Eds), p. 127. M. Dekker, New York 1997.
22. LaPierre R. B., Rohrmann A. C., Schlenker J. L., Wood J. D., Rubin M., Rohrbach W. J.: *Zeolites* **1985**, *5*, 3346.
23. Fyfe C. A., Gies H., Kokotailo G. T., Marler B., Cox D. E.: *J. Phys. Chem.* **1990**, *94*, 3718.
24. Ritsch S., Ohnishi N., Ohsuna T., Hiraga K., Terasaki O., Kubota Y., Sugi Y.: *Chem. Mater.* **1998**, *10*, 3958.
25. Mitra A., Kirby C. W., Wang Z., Huang L., Wang H., Huang Y., Yan Y.: *Microporous Mesoporous Mater.* **2002**, *54*, 175.
26. Perego C., Amarilli S., Millini R., Bellussi G., Girotti G., Terzoni G.: *Microporous Mater.* **1996**, *6*, 395.
27. Wichterlová B., Čejka J., Žilková N.: *Microporous Mater.* **1996**, *6*, 405.
28. Zhang W., Smirniotis P. G.: *Catal. Lett.* **1999**, *60*, 223.
29. Reddy K. M., Moudrakovski I., Sayari A.: *J. Chem. Soc., Chem. Commun.* **1994**, 1491.
30. Bhaumik A., Dongare M. K., Kumar R.: *Microporous Mater.* **1995**, *5*, 173.
31. Mal N. K., Bhaumik A., Kumar R., Ramaswamy A. V.: *Catal. Lett.* **1995**, *33*, 387.
32. Coudurier G., Naccache C., Vedrine J. C.: *J. Chem. Soc., Chem. Commun.* **1982**, 1413.
33. Kotrla J., Kubelkova L., Lee C. C., Gorte R. J.: *J. Phys. Chem. B* **1998**, *102*, 1437.
34. Emeis C. A.: *J. Catal.* **1993**, *141*, 347.
35. Čejka J., Košová G., Žilková N., Hrubá I.: *Stud. Surf. Sci. Catal.* **2002**, *142*, 247.
36. Flanigen E. M., Khatami H., Szymanski H.: *Adv. Chem. Ser.* **1971**, *101*, 201.
37. Sozstak R.: *Molecular Sieves, Principles of Synthesis and Identification*, 2nd ed., p. 89. Blackie Acad. & Prof., London 1998.
38. Lunsford J. H.: *J. Phys. Chem.* **1968**, *72*, 4163.
39. Mirodatos C., Barthomeuf D.: *J. Chem. Soc., Chem. Commun.* **1981**, 39.
40. Čejka J., Vondrová A., Wichterlová B., Jerschkewitz H., Lischke G., Schreier E.: *Collect. Czech. Chem. Commun.* **1995**, *60*, 412.
41. Chiche B. H., Dutartre R., di Renzo F., Fajula F., Katovic A., Regina A., Giordano G.: *Catal. Lett.* **1995**, *31*, 359.
42. Chu C. T.-W., Chang C. D.: *J. Phys. Chem.* **1985**, *89*, 1569.
43. Čejka J., Dědeček J., Kotrla J., Tudor M., Žilková N., Ernst S.: *Stud. Surf. Sci. Catal.* **2001**, *135*, 14-P-21.
44. Zecchina A., Bordiga S., Spoto G., Scarano D., Petrini G., Leofanti G., Padovan M., Otero Arran C.: *J. Chem. Soc., Faraday Trans.* **1992**, *88*, 2959.
45. Chen J., Thomas J. M., Sankar G.: *J. Chem. Soc., Faraday Trans.* **1994**, *90*, 3455.
46. Zhang W., Smirniotis P. G., Gangoda M., Bose R. N.: *J. Phys. Chem. B* **2000**, *104*, 4122.

47. Kunkeler P. J., Zuurdeeg B. J., van der Waal J. C., van Bokhoven J. A., Koningsberger D. C., van Bekkum H.: *J. Catal.* **1998**, *180*, 234.
48. Bourgeat-Lami E., Massiani P., di Renzo F., Espiau P., Fajula F., des Courieres T.: *Appl. Catal.* **1991**, *72*, 139.